Electronic Supplementary Material
for
High-Performance Carbon Nanotube Electronic Ratchets

Ji Hao,[1] Sanjini U. Nanayakkara,[2] Eric J. Tervo,[1] Jeffrey L. Blackburn,[2] and Andrew J. Ferguson[1,*]

[1]Chemistry and Nanoscience Center, National Renewable Energy Laboratory, Golden, CO 80401, USA
[2]Materials Science Center, National Renewable Energy Laboratory, Golden, CO 80401, USA

TABLE OF CONTENTS

S1. Optical Characterization of Enriched s-SWCNT Samples

Diameter Distribution Extracted from Kataura Analysis of Enriched s-SWCNT Ink

Figure S1 illustrates the 'Kataura analysis' for the enriched arc discharge s-SWCNT ink, where the absorbance peak envelopes for the first (S_{11}) and second (S_{22}) excitonic transitions are mapped onto 'Kataura plots' that correlate the energies of these transitions to s-SWCNT diameter, which suggests a diameter distribution of ca. 1.15 nm to 1.95 nm. Information about the specific distribution of chiral indices in our samples requires two-dimensional photoluminescence excitation mapping, which is beyond the scope of this study. The absence of distinctive absorbance peaks between the absorbance peak envelopes for the second (S_{22}) and third (S_{33}) excitonic transitions indicates that there is a negligible amount of metallic SWCNTs in our ink.

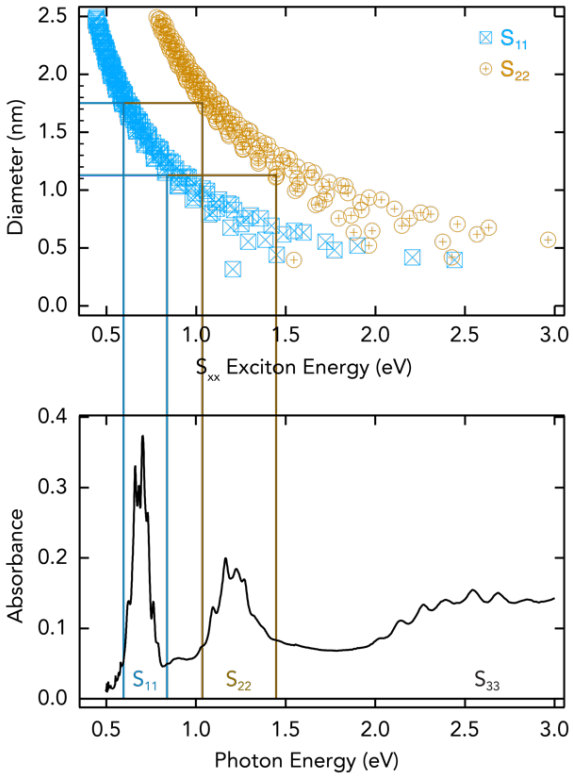

Figure S1. Kataura Analysis of Enriched s-SWCNT Ink Absorbance Spectrum

By mapping the absorbance peak envelopes for the first (S_{11}) and second (S_{22}) excitonic transitions in the absorbance spectrum (bottom) to the 'Kataura plot' of the diameter vs. exciton energy (top), the diameter distribution of carbon nanotubes can be extracted for an enriched s-SWCNT ink.

Pristine and Doped s-SWCNT Networks

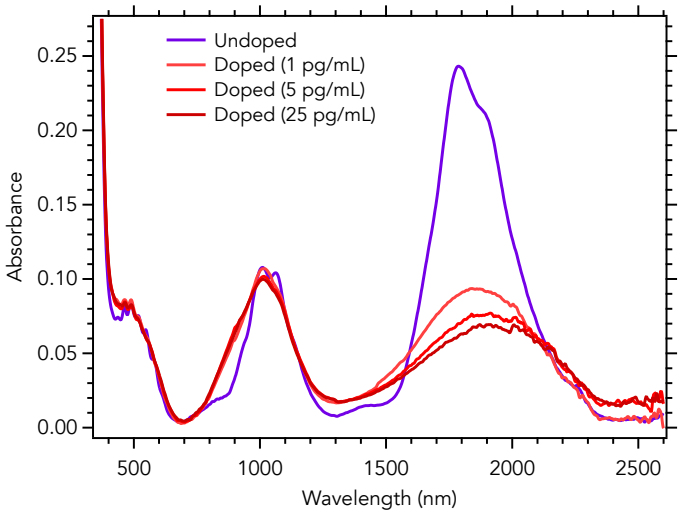

Figure S2. Optical Properties of Pristine and Doped s-SWCNT Networks
Absorbance spectra of the undoped s-SWCNT thin film network and equivalent networks as a function of p-type doping with three different OA concentrations.

S2. Characterization of s-SWCNT Transistors

Optical Micrographs

Figure S3 shows optical micrographs of several s-SWCNT electronic ratchets based on a simple field-effect transistor (FET) geometry. Figure S3a shows the blank FET substrate, whereas Figures S3b and S3c illustrate the pristine s-SWCNT device and a s-SWCNT device that has been pre-patterned by partially covering the transistor channel with photoresist (Microchem S1818).

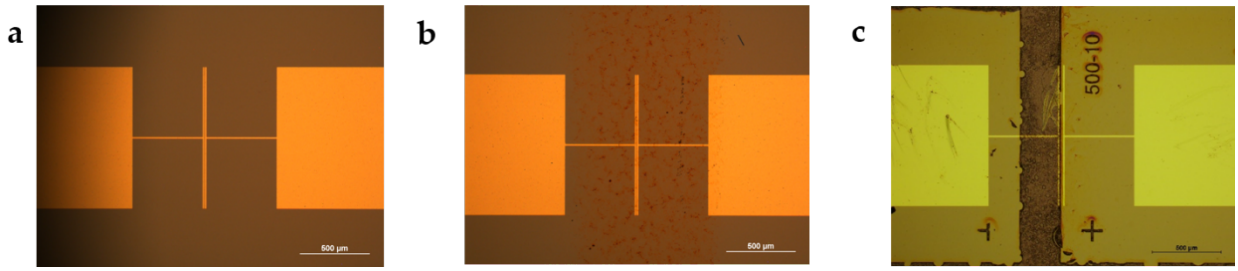

Figure S3. Optical Micrographs of s-SWCNT Electronic Ratchets
(a) Blank field-effect transistor (FET) substrate, (b) pristine s-SWCNT device, and (c) pre-patterned s-SWCNT device partially covered with photoresist.

Field-effect Transistor Transport Measurements

Transport measurements were performed in a helium-filled glovebox, using Keithley 2400 source-measure units (SMU) controlled with a laptop running a custom LabVIEW program to perform the measurement and collect experimental data. The typical current-voltage (I-V) measurement was performed using a single Keithley 2400 SMU connected to the source and drain contacts. Typical field-effect transistor measurements were performed by using two Keithley 2400 SMUs, where one Keithley 2400 SMU was used to supply the source-drain voltage and monitor the source-drain current and the other was used to supply the gate voltage and monitor the gate-channel current. The typical applied source-drain bias (V_{SD}) is 0.1 V, and the gate voltage is swept over the range −40 V to +30 V with

an ca. 0.7 V increment. The carrier mobility was calculated by the standard equation: $\mu_p = \frac{\partial I_{SD}}{\partial V_G} \frac{1}{V_{SD}} \frac{1}{C_{ox}} \frac{L_{CH}}{W_{CH}}$, where C_{OX} is the oxide capacitance per unit area of SiO_2 gate dielectric layer.

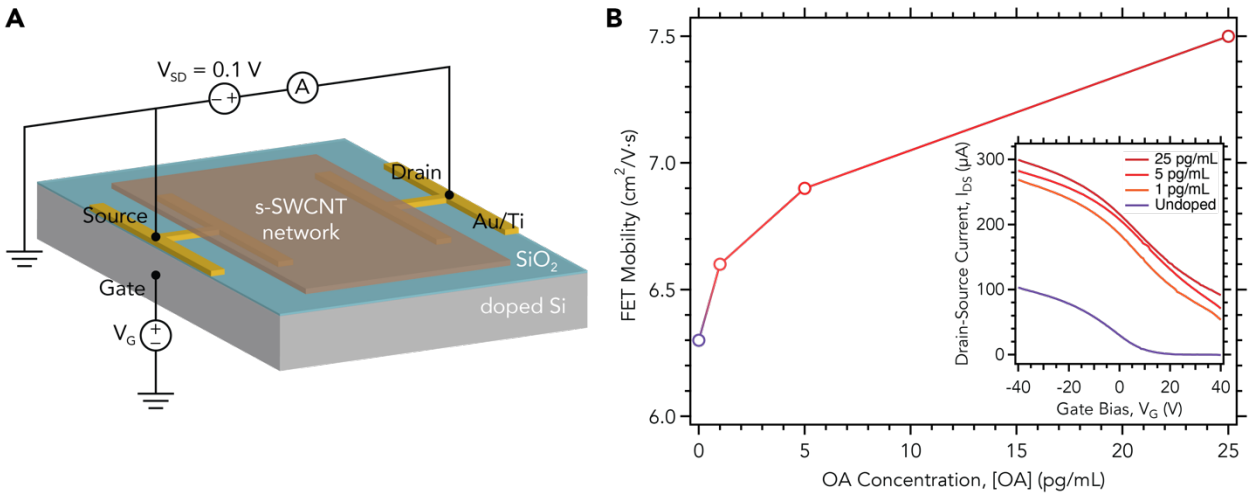

Figure S4. s-SWCNT Field-effect Transistor Devices

(A) Schematic of the field-effect transistor (FET) device configuration for electronic ratchet measurements. (B) The dependence of the field-effect mobility, extracted from the output curves (inset), on the concentration of OA used during the doping step.

S3. Additional Characterization of s-SWCNT Electronic Ratchets

s-SWCNT Electronic Ratchet Architectures

The as-deposited 'undoped' s-SWCNT transistors (Figure S5A) are not intentionally doped with redox molecules, but are likely (lightly) *p*-type, presumably by adventitious adsorption of oxygen or water molecules onto the surface of the nanotubes. 'Doped' s-SWCNT transistors (Figure S5B) are intentionally and homogeneously doped *p*-type with the one-electron oxidant triethyloxonium hexachloroantimonate, OA (Figure 1B in the main manuscript). The asymmetry in the device is generated by applying a voltage stress to the drain electrode, $V_D = -15$ V, for 10 minutes. Pre-patterned s-SWCNT transistors (Figure S5C) are created by protecting the one portion of the channel with a photolithographically patterned photoresist and subsequent doping of the other portion of the channel with OA to create a homojunction (p/p^+) near the center of the channel, and these devices are labeled 'built-in junction'.

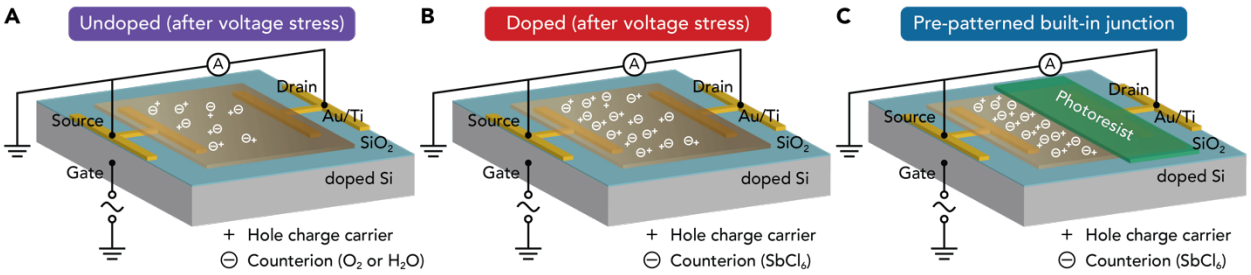

Figure S5. Electronic Ratchet Device Architectures

Schematic architectures of the (A) 'undoped' (adventitiously doped) and (B) intentionally 'doped' electronic ratchets after voltage stress, and (C) the pre-patterned 'built-in junction' electronic ratchet.

Undoped (Adventitiously Doped) s-SWCNT Electronic Ratchets

In the case of the adventitiously doped device, the voltage stress applied to the drain electrode, $V_D = -15$ V for 10 minutes, results in non-linear current-voltage behavior (Figure S6A), indicative of a spatial asymmetry within the FET channel.

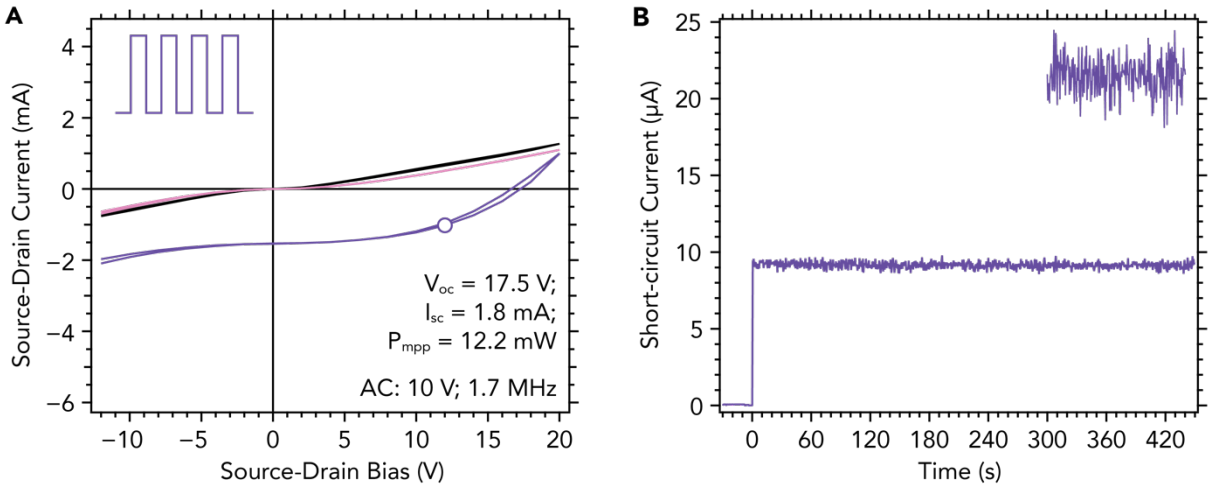

Figure S6. Adventitiously Doped s-SWCNT Electronic Ratchet Devices

(A) Two-terminal current-voltage curves, illustrating the rectifying behavior under a square wave bias applied to the gate electrode and (B) short-circuit current output under application of a simulated electrical noise signal applied to the gate electrode, for an adventitiously doped carbon nanotube ratchet devices following voltage stress.

Dependence of the Electronic Ratchet Output on the FET Charge-Carrier Mobility

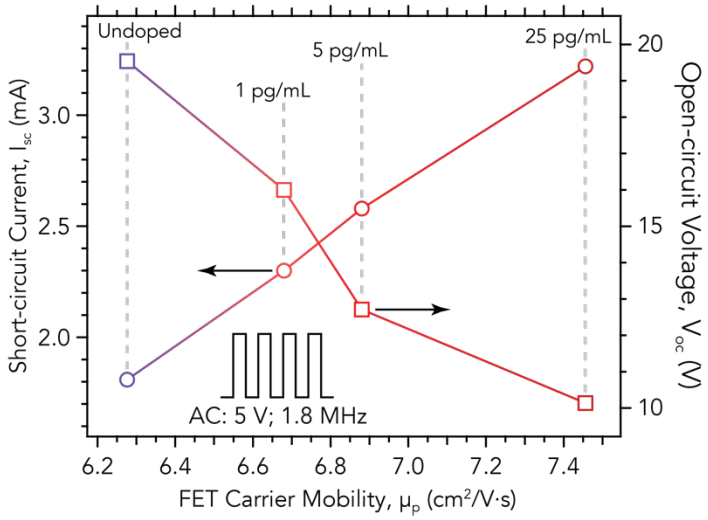

Figure S7. Dependence of the Electronic Ratchet Device Parameters on Charge-Carrier Mobility

(left axis) Short-circuit current, I_{sc}, and (right axis) open-circuit voltage, V_{oc} as a function of the field-effect carrier mobility in the s-SWCNT network (V_a = 10 V; f = 1.8 MHz), for the undoped electronic ratchet and devices p-type doped with three different OA concentrations.

Dependence of the Electronic Ratchet Performance on the Gate Signal Amplitude

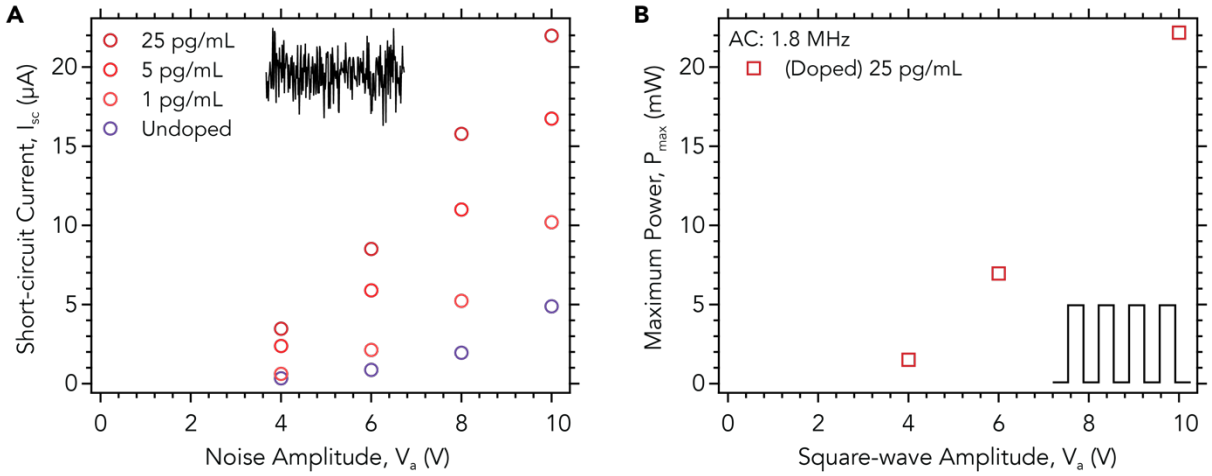

Figure S8. Electronic Ratchet Performance as Function of the Gate Signal Amplitude

(A) Short-circuit current, I_{sc}, as a function of the amplitude of the simulated electronic noise signal applied to the gate electrode. (B) Peak power, P_{max}, for the electronic ratchet p-type doped at an OA concentration of 25 pg/mL as a function of the amplitude of the square waveform AC signal applied to the gate electrode (f = 1.8 MHz).

Organic Electronic Ratchet Stability

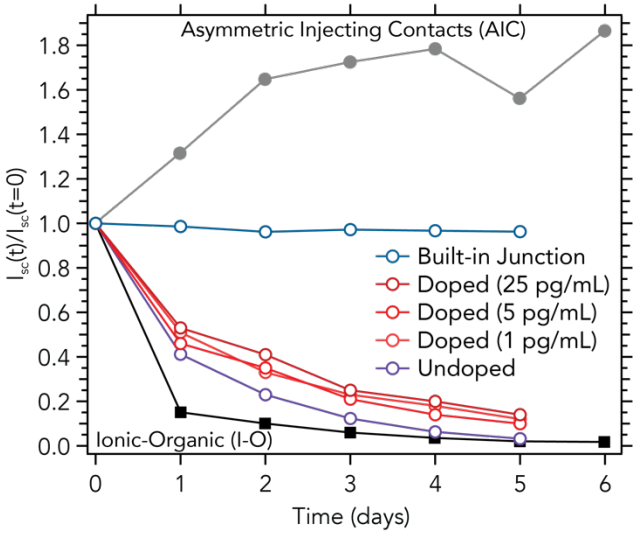

Organic Electronic Ratchet Type		Starting Current (μA)	Change (%)	Residual Current (μA)
Polymer	Asymmetric Contacts	1.18	+56	1.84
		2.31		3.60
	Ionic-Organic	25.3	–98	0.51
		96.7		1.93
s-SWCNT	Built-in Junction	1530	–4	1470
	Doped (25 pg mL^{-1})	3300	–86	462
	Doped (5 pg mL^{-1})	2580	–90	258
	Doped (1 pg mL^{-1})	2310	–88	277
	Undoped	1800	–97	54

Figure S9. Comparison of Stability of s-SWCNT and Polymer-based Electronic Ratchet

(left) A plot of the time-dependence of the short-circuit current, I_{sc}, normalized to the I_{sc} at time t=0 and (right) A table illustrating the impact of device performance degradation on the output I_{sc} after 5 days (i.e., the final point in our time series) for the various s-SWCNT electronic ratchet devices prepared in this work, compared to those for polymer-based electronic ratchets with either asymmetric injecting contacts (AIC) or polymer-based ionic-organic (I-O) ratchets. Data for the polymer-based devices was estimated and extracted from Huang, J. *et al.* "Solution-Processed Ion-Free Organic Ratchets with Asymmetric Contacts." *Adv. Mater.* **30**, 1804794 (2018) https://doi.org/10.1002/adma.201804794 and Hu, Y. *et al.* "Understanding the Device Physics in Polymer-Based Ionic–Organic Ratchets." *Adv. Mater.* **29**, 1606464 (2017). https://doi.org/10.1002/adma.201606464

Dependence of the Electronic Ratchet Output on the FET Channel Length

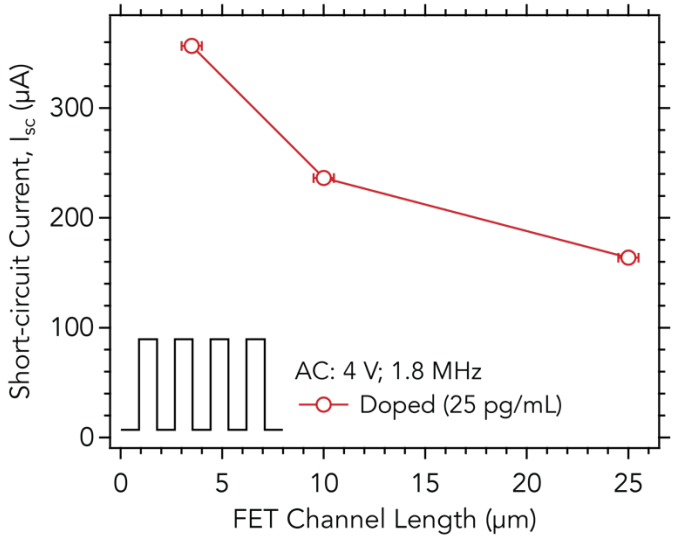

Figure S10. Dependence of the Electronic Ratchet Current Output on the FET Channel Length
Short-circuit current, I_{sc} for the electronic ratchet p-type doped at an OA concentration of 25 pg/mL as a function of the field-effect transistor channel length for a square waveform AC signal applied to the gate electrode (V_a = 4 V; f = 1.8 MHz).

Comparison of Experimental Organic Electronic Ratchet Studies

Table S1: Comparison of semiconducting single-walled carbon nanotube electronic ratchets with previously published polymer-based electronic ratchets

	Field-effect Transistors		**Electronic Ratchets**								
			Measurement Parameters					**Optimum Ratchet Performance**			
Channel Material	Channel Length (μm)	FET Mobility ($cm^2\ V^{-1}\ s^{-1}$)	Pulse/Function Generator	Contact Architecture	Channel Length (μm)	Applied Gate Voltage Amplitude (V)[g]	Frequency (MHz)[h]	Short-circuit Current, I_{sc} (μA)	Open-circuit Voltage, V_{oc} (V)	Maximum Power, P_{max} (mW)	Ref
P3HT[a]	80	0.02	Keithley 4200 PG2	Symmetric	10	10	5	2.6	3.38	0.002	1
PCDTPT[b]	20	0.4-0.5	Keithley 4200 PG2	Symmetric	20	10	5	25.3	8.11	0.052	2
			Tektronix AFG320				13.56[i]	96.7	6.5	0.169	
	65	0.03-0.06	Keithley 4200 PG2	Asymmetric	57	10	0.04	1.18	17.1	0.00911	3
					32		0.163	2.31	12.9	0.0114	
PCBM[c]	60	0.07-0.15	Keithley 4200 PG2	Symmetric	60	10	5	7.29	-6.06	0.0125	4
SWCNT[d]	4	6.3	Agilent 33220A	Symmetric	4	10	1.7	1800	17.5	11.8	This work
SWCNT[e]		6.7					1.8	2310	16	15.4	
		6.9						2580	12.7	18.6	
		7.5						3300	11.2	14.3	
SWCNT[f]	25	4.75			25		2.2	1530	8.3	3.53	

[a] P3HT = poly(3-hexylthiophene-2,5-diyl) (Sigma–Aldrich Plexcore OS 1200);

[b] PCDTPT = poly(4-(4,4-dihexadecyl-4*H*-cyclopenta[1,2-*b*:5,4-*b*']dithiophen-2-yl)-*alt*-[1,2,5]thiadiazolo[3,4-*c*]pyridine;

[c] PCBM = phenyl-C_{61} butyric acid methyl ester (Solenne BV).

SWCNT = semiconducting single-walled carbon nanotubes extracted from raw arc discharge carbon nanotube soot (Sigma-Aldrich; SKU 698695; Lot#MKBC7933V) using poly[(9,9-dioctylfluorenyl-2,7-diyl)-*alt*-*co*-(6,6'-{2,2'-bipyridine})] (PFO-BPy; ADS153UV; Lot #161002A1; M_w = 55 kDa).

[d] 'undoped' device adventitiously doped with adsorbed, atmospheric O_2 or H_2O.

[e] devices intentionally 'doped' using triethyloxonium hexachloroantimonate (OA; Sigma-Aldrich).

[f] patterned devices partially doped with OA to create a 'built-in junction'.

[g] The quoted voltage amplitude is double the nominal voltage setting used on the pulse/function generator. These pulse/function generators typically source a voltage that will be split (i.e., half the voltage bias will be experienced by the sample) under 'impedance matching' conditions. However, the impedance of the ratchet devices is significantly larger than the standard output impedance of 50 Ω, meaning that the experiments are conducted under 'impedance bridging' conditions where the entire voltage sourced by the pulse/function generator is applied to the gate electrode of the ratchet architecture.

[h] AC square wave applied to gate (unless otherwise noted).

[I] AC sine wave applied to gate.

REFERENCES

1. O. V. Mikhnenko, S. D. Collins and T.-Q. Nguyen, *Adv. Mater.*, 2015, **27**, 2007-2012.
2. Y. Hu, V. Brus, W. Cao, K. Liao, H. Phan, M. Wang, K. Banerjee, G. C. Bazan and T.-Q. Nguyen, *Adv. Mater.*, 2017, **29**, 1606464.
3. J. Huang, A. Karki, V. V. Brus, Y. Hu, H. Phan, A. T. Lill, M. Wang, G. C. Bazan and T.-Q. Nguyen, *Adv. Mater.*, 2018, **30**, 1804794.
4. K. Liao, S. D. Collins, V. V. Brus, O. V. Mikhnenko, Y. Hu, H. Phan and T.-Q. Nguyen, *ACS Appl. Mater. Interfaces*, 2019, **11**, 1081-1087.